

Evaluation of x-ray diffraction enhanced imaging in the diagnosis of breast cancer

Chenglin Liu^{1,2}, Xiaohui Yan¹, Xinyi Zhang^{1,3}, Wentao Yang⁴,
Weijun Peng⁴, Daren Shi⁴, Peiping Zhu⁵, Wanxia Huang⁵ and
Qingxi Yuan⁵

¹ Synchrotron Radiation Research Center, Physics Department, Surface Physics Laboratory (National Key Laboratory) of Fudan University, Shanghai 200433, People's Republic of China

² Physics Department of Yancheng Teachers' College, Yancheng 224002, People's Republic of China

³ Shanghai Research Center of Acupuncture and Meridian, Pudong, Shanghai 201203, People's Republic of China

⁴ Cancer Hospital, Medical Center of Fudan University, Shanghai 200032, People's Republic of China

⁵ Beijing Synchrotron Radiation Facility, Institute of High Energy Physics, Chinese Academy of Sciences, Beijing 100039, People's Republic of China

E-mail: xy-zhang@fudan.edu.cn

Received 8 March 2006, in final form 20 August 2006

Published 29 December 2006

Online at stacks.iop.org/PMB/52/419

Abstract

The significance of the x-ray diffraction enhanced imaging (DEI) technique in the diagnosis of breast cancer and its feasibility in clinical medical imaging are evaluated. Different massive specimens including normal breast tissues, benign breast tumour tissues and malignant breast tumour tissues are imaged with the DEI method. The images are recorded respectively by CCD or x-ray film at different positions of the rocking curve and processed with a pixel-by-pixel algorithm. The characteristics of the DEI images about the normal and diseased tissues are compared. The rocking curves of a double-crystal diffractometer with various tissues are also studied. The differences in DEI images and their rocking curves are evaluated for early diagnosis of breast cancers.

(Some figures in this article are in colour only in the electronic version)

1. Introduction

Breast diseases are common for women and breast cancer is a dangerous killer (Bothorel *et al* 1997). Early diagnosis and treatment are the best ways to reduce the hazard. Current procedures for the diagnosis of breast cancer mainly include self-examination, mammography (Feig 2002, Freedman *et al* 2003, Humphrey *et al* 2002), ultrasonography (US) (Shankar

et al 1993) and magnetic resonance imaging (MRI) (Orel *et al* 1997). Mammography is currently recognized as the gold standard for the early detection of breast cancer because it requires lower radiation doses, though the rate of false negatives is still as high as 10 per cent (Wilkinson *et al* 2005). Recently, some new techniques, such as digital mammography, computer aided diagnosis, synchrotron mammography and digital tomosynthesis have been developed to optimize image quality and improve the diagnostic capabilities (Giammarile and Bremond 2004, Niklason *et al* 1997). The synchrotron radiation, which is electromagnetic radiation emitted by charged particles moving with a speed very close to light speed in a circular orbit, was first found in 1947 and then widely used in different fields, including material science, biology, medicine (Margaritondo and Meuli 2003, Suortti and Thomlinson 2003), etc. Images obtained by using synchrotron radiation with higher spatial resolution and better contrast (Fiedler *et al* 2003) are superior to those with a conventional x-ray source. With synchrotron radiation, some microstructures inside organic tissues can be shown, which are often missed with conventional techniques.

Since the middle of the 1990s, x-ray phase-contrast imaging techniques, which can clearly show the microstructure of biological soft tissues under low radiation dose, have been quickly developed (Lewis *et al* 2002). Diffraction enhanced imaging (DEI), whose contrast comes from the absorption, the refractive gradient and the small-angle scattering rejection (usually called extinction), is one of them (Hasnah *et al* 2002, Zhong *et al* 2000). The DEI method enhances the sharpness and clarity of the soft tissue image relative to the traditional method due to the combination of more contrast mechanisms (Menk 1999). In recent years, DEI has shown some latent applications in early diagnosis (Lewis 2004). The spatial resolution of DEI images is higher than that of B-mode ultrasound, MRI or CT (computer tomography), and reaches the order of micrometres (Liu *et al* 2005). The combination of DEI and CT (also called DEI-CT) makes medical images of tumours extraordinarily similar to pathological histology (Fiedler *et al* 2004). Moreover, due to the high intensity of synchrotron radiation, only a short exposure time (see below) is needed. Therefore, synchrotron radiation based DEI has a low risk of complications due to the radiation exposure which is obviously an advantage in the early diagnosis of cancer.

In this paper, we compared various DEI images of the tissues for the normal breast, benign breast tumour and malignant breast tumour along with their rocking curves to distinguish the microstructures inside those tissues, and we also discussed the merits of this technique for medical applications.

2. Materials and methods

The specimens were prepared in the Cancer Hospital, Medical Center of Fudan University. We selected 13 of them, including four cases of normal breast tissue, four cases of benign breast tumour tissue and five cases of breast cancer tissue. Both the diseased tissues and the healthy ones were taken from mastectomy sufferers. The main part of each cancer tissue included a great mass of cancer nests, and the normal tissue was taken from a distance of about 2 cm beside the tumour. These specimens were cut into small pieces of 10×9 mm with a thickness of approximately 2 mm and fixed in 10% buffered formalin.

The DEI experiments have been carried out at the topography end station of the 4W1A beamline of the Beijing Synchrotron Radiation Facility (BSRF). The energy of the monochromatic x-rays was 9 keV with an incident angle of 12.7° , and the maximum size of the light spot was approximately 12×10 mm² at the position of specimen. The analyser was fixed at the axis so it could be tuned to get the different positions of the rocking curve. The DEI images were recorded using a CCD with 1300×1030 pixels (X-ray Fast Digital Imager

18 mm system, Photonic-science Ltd, UK) or industrial x-ray film (Fuji IX80) behind the analyser crystal. The spatial resolutions of the CCD and x-ray film (pixel sizes) were $10.9 \mu\text{m}$ and $2.3 \mu\text{m}$, respectively. The distance between the specimen and CCD detector was about 1 m. The photon flux incident onto the specimens is proportional to the beam current. Hence we can use the product of beam current multiplied by the exposure time as the exposure dose. In our experiments the exposure dose was controlled as a constant, whose average values were about 26.4 mA s and 360 mA s for the CCD and x-ray film, respectively. The beam current was normally between 50 and 100 mA and the exposure time ranged from less than 1 s to several seconds.

For the DEI setup in the BSRF, two Si (1 1 1) crystals are equipped. One serves as a monochromator and the other one serves as the analyser. These two crystals formed a double-crystal diffractometer. The rocking curve, which is the relationship between the reflected intensity and deflection angle of the analyser, can be obtained by tuning the analyser continuously to different angles related to the Bragg angle of Si (1 1 1). The variation of the rocking curve with different breast tissues has been carefully studied.

When the CCD is used as the detector, three kinds of images can be obtained. The first one is recorded at the peak position of the rocking curve, which is usually called the peak image. The other two images are taken when the analyser is tuned to the FWHM (full-width of half-maximum) positions on the either side of the rocking curve. These two images contain the same absorption and little scattering information but opposite refraction information. When these two images are added pixel by pixel, the refraction information will be eliminated, thus we can obtain an image called the apparent absorption image because of the pure absorption contrast (but with weak extinction). When two images are subtracted pixel by pixel, the so-called refraction image can be obtained, in which not only the refraction but also the absorption contrast is included. And consequently the edge effect will be greatly enhanced. This image processing is very easy because only a simple pixel-by-pixel algorithm is needed.

In addition, we also recorded the images by x-ray films and read them out through an optical microscope. In this case two different imaging setups were used. One is to place the x-ray film about 1 cm behind the sample without using the analyser crystal, and record the image, which is called absorption image, resembling conventional mammography. The other setup is to place the x-ray film just behind the analyser crystal which is in the top position of its rocking curve, and obtain the peak image. These images will display some microstructures of various tissues after they are read out by the optical microscope.

3. Results

In our DEI experiments, we obtained various images from those tissues. The various normal tissue (or benign or malignant tumour tissue) cases had similar characteristics in their DEI images. Therefore, only one set of DEI images from each case is shown here. We compared these images to evaluate the significance of the DEI method and show the differences between the normal, benign and malignant tissues.

The peak image recorded by CCD of these three different kinds of tissues, normal, benign tumour and malignant tumour, are shown in figure 1. They contain the information of absorption and small-angle scattering rejection (extinction). The apparent absorption images (figure 2) and the refraction images (figure 3) are obtained by the simple pixel-by-pixel algorithm (Chapman *et al* 1997) using two images obtained as the analyser is tuned to either side of the FWHM positions, i.e. the low-angle position and the high-angle position of the rocking curve, as mentioned above. The refraction image is extraordinarily sensitive to the

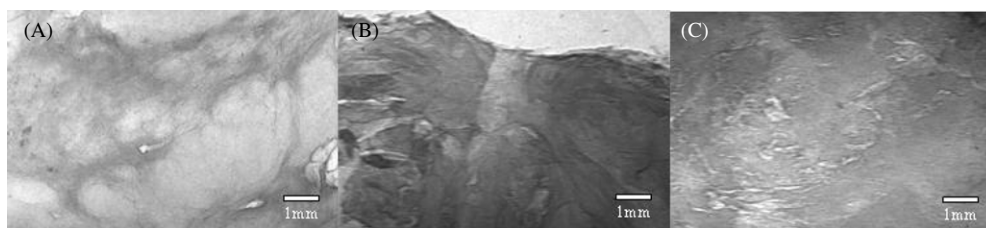


Figure 1. Peak images which are recorded by CCD at the peak position of rocking curves of different breast tissues (A) normal, (B) benign tumour, and (C) malignant tumour).

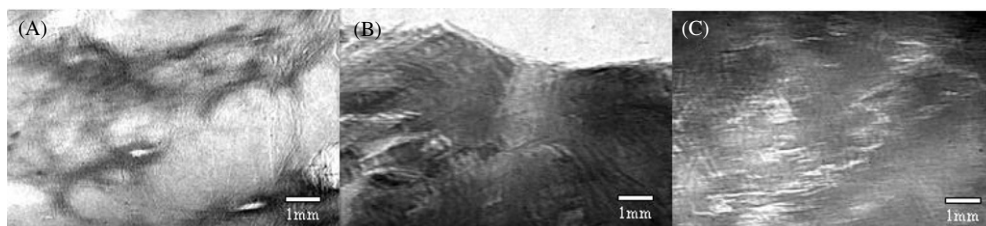


Figure 2. Apparent absorption images of different breast tissues. These images are obtained by adding two raw images pixel by pixel. The raw images are recorded by CCD when the analyser is tuned to either side of the FWHM positions. (A) normal, (B) benign tumour, and (C) malignant tumour).

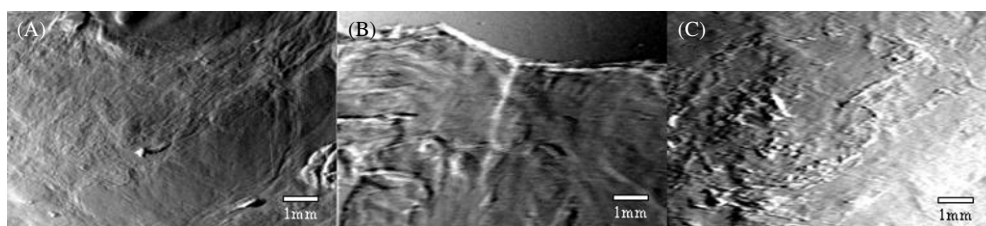


Figure 3. Refraction images of different breast tissues. These images are obtained by subtracting two raw images by pixel by pixel. The raw images are recorded by CCD when the analyser is tuned to either side of the FWHM positions. (A) normal, (B) benign tumour, and (C) malignant tumour).

variation of the refractive index of the sample. A few microstructures of tissues can be seen in those images. Especially, there are evidently differences in the calcification between the normal tissues, benign and malignant tumour tissues (see discussion section below).

In order to compare diffraction enhanced imaging with the conventional radiographs, x-ray films were used as the detector. The peak images were recorded by x-ray films as shown in figure 4. The absorption images are shown in figure 5, and as we mentioned earlier, in this case the analyser crystal was not used. The contrast of the absorption images is lower than that of the peak images due to the strong scattering which will reduce the image's quality. When the peak images are magnified by the optical microscope, some microstructures can be clearly seen. For example, we can see bundles which consist of fibres of about $30\ \mu\text{m}$ in diameter (denoted by the black arrow) and some reticulate structures (by the white arrow) in figure 6(A). Some small cavities are shown by arrows in figure 6(B). In the same way, the



Figure 4. Peak images which are recorded by x-ray films at the peak position of rocking curves of different breast tissues (A) normal, (B) benign tumour, and (C) malignant tumour).



Figure 5. Absorption images which are recorded by x-ray films of different breast tissues (A) normal, (B) benign tumour, and (C) malignant tumour).

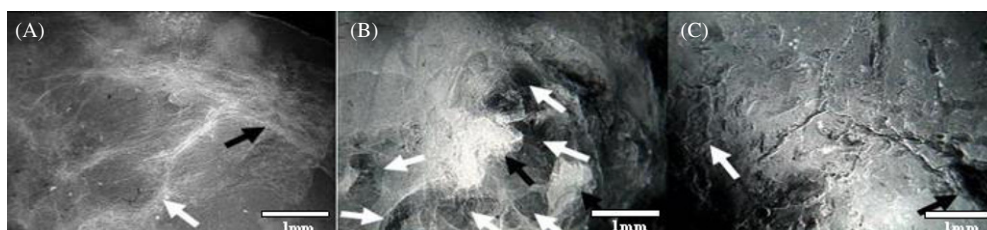


Figure 6. Peak images of various breast tissues recorded by industrial x-ray films at the peak position of the rocking curve and magnified by an optical microscope. These images can show the microstructures of various breast tissues (A) normal, (B) benign tumour, and (C) malignant tumour).

irregular conglomeration (pointed out by the white arrow) and the expanded duct (by the black arrow) can be also observed, as shown in figure 6(C).

On the other hand, the rocking curve can also show the differences of various tissues in the DEI method. Figure 7 shows the rocking curves of the double-crystal diffractometer itself with different breast tissues. Comparing these rocking curves, the diversities of peak displacement and FWHM are not obvious. However, the intensity and integrated intensity of reflectivity can show definite differences. These values for each case and their average values are collected in table 1.

4. Discussion

4.1. Peak image, apparent absorption image and refraction image

There are three kinds of images which can be used in the diagnosis of breast tumours. These images are peak images, apparent absorption images and refraction images. The peak image

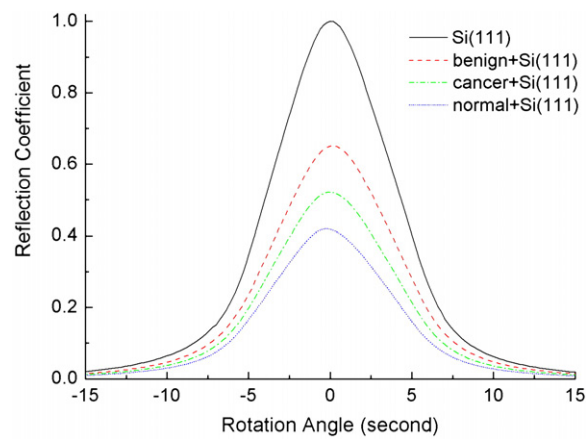


Figure 7. Rocking curves of the double-crystal diffractometer including various breast tissues taken with the 9 keV x-ray. There are obvious differences between these rocking curves taken with or without various tissues.

Table 1. The peak displacement, reflected intensity and FWHM of the rocking curve of the double-crystal diffractometer with different breast tissues and 9 keV x-ray.

	Peak displacement (s)	FWHM (s)	Reflected intensity	Integrated intensity
Double-crystal diffractometer	0.00	8.37	1.00	8.37
Normal breast tissue +	0.2	8.96	0.381	3.87
double-crystal diffractometer	0.2 (0.25 ± 0.08) ^a	8.97 (9.00 ± 0.06)	0.332 (0.43 ± 0.07)	
	0.2	9.13	0.522	
	0.4	8.96	0.477	
Benign breast tumour tissue +	-0.2	9.18	0.498	6.05
double-crystal diffractometer	0.0 (-0.15 ± 0.08)	9.17 (9.16 ± 0.08)	0.763 (0.66 ± 0.09)	
	-0.2	9.00	0.734	
	-0.2	9.30	0.633	
Breast cancer tissue +	0.2	8.80	0.594	4.49
double-crystal diffractometer	0.0 (0.00 ± 0.16)	8.97 (8.97 ± 0.07)	0.392 (0.50 ± 0.10)	
	-0.2	9.14	0.413	
	0.2	8.97	0.567	
	-0.2	8.96	0.678	

^a Data in parentheses are the average values.

can provide the absorption and extinction information. Its contrast will not be seriously affected by the scattering because those scatters are out of the rocking curve, which is the extinction effect. In other words, the small-angle scattering is rejected from the peak images. The contrast of peak images can be enhanced by virtue of the extinction effect. Therefore, some new structures will be seen in the peak images. For example, the fibril of normal breast tissue with a diameter of about 30 μm (see figure 1(A)), the benign tumour with a sharp edge (see figure 1(B)) and the sheets of calcifications (formed by calcified spots of tens of micrometres) of malignant breast tissue (see figure 1(C)) are shown in those peak images.

The apparent absorption images shown in figure 2 are similar to the conventional x-ray image and there are no advantages in distinguishing the microstructure of soft tissues. Its clarity is worse than that of the peak image because it contains a weak small-angle scattering signal besides absorption. Nevertheless, some structures can still be found in apparent absorption images. For example, the boundaries of the breast gland and the reticulate structure are clearly seen in normal breast tissues as shown in figure 2(A). As for the benign tumour, the boundary of the tumour is not obvious because the density of benign tumour is similar to the environmental tissue (see figure 2(B)). A few calcifications can be distinctly seen in figure 2(C) from the breast cancer tissues.

Some typical refraction images of various breast tissues are shown in figure 3. In figure 3(A), the boundary of the fat, the fibril and the gland of normal breast tissue can be seen clearly. For benign tumours, the ellipsoidal and sheet-like masses of tumours are shown in figure 3(B). The fibre bundle of tens of micrometres in diameter and two 1 to 2 millimetre sized masses can be seen. For breast cancer the calcification is the most familiar symptom. Some circinal or anomalous trigonal or linear calcifications of breast cancer are shown in figure 3(C). The size of these calcifications ranges from 50 to 200 micrometres, respectively. The linear calcification, which is assembled from many calcified spots and distributed along the breast duct, is the most important diagnostic standard. Accordingly, there are important values of the DEI method in diagnosing breast cancer because some linear or branched calcifications can be clearly seen in refraction images. They are so valuable that we can directly see the inside structure of soft tissues without the need of large numbers of pathology slices and thus much diagnosing work with optical microscopes can be avoided. The refraction image contains abundant structural information; therefore we can use it to distinguish benign and malignant breast tumours.

4.2. Peak image and absorption image recorded by x-ray films

X-ray films are used instead of CCDs to record the image because the spatial resolution of x-ray film is higher than that of the CCD. If the x-ray film is placed directly behind the sample without the analyser crystal, the recorded image is called the synchrotron based absorption image. It strongly resembles mammography, and contains a large number of scattering signals. The quality of such absorption images (see figure 5) is superior to those obtained from medical x-ray tubes due to the high intensity of the synchrotron radiation, but their contrast cannot be improved because there is no extinction contrast in these images. As a result, the fine structure of normal tissue does not emerge, the edge of benign tumour is blurry, and the profile of calcifications is not that obvious.

For peak images recorded by the x-ray film placed behind the analyser crystal, the clarity and contrast can be improved. Some microstructures of various tissues which do not display in the absorption images can be seen. Similar to the peak images from CCD (see figure 1), fibre reticulation of normal breast tissue, fibre bundles of benign breast tumour and linear calcification can be seen in the peak images recorded by the x-ray films (see figure 4).

4.3. Peak image read by the optical microscope

The clarity of images can be further improved if the peak images recorded by the industrial x-ray film are read out by an optical microscope. Some microstructures in breast tissues can be seen in these images. For normal breast tissues, their fibres of about 30 μm in diameter are enlaced into bundles (denoted by the black arrow in figure 6(A)) and form the reticulate structures (by the white arrow in figure 6(A)). There are small bright spots which

are calcifications in the normal breast tissues because of calcium salt deposited in the ageing breast tissue. The fibres of benign tumour breast tissue are in disorder and make up anomaly masses (see figure 6(B)), which means the high density tumour tissues get together and form anomalous conglomerations. The sizes of the conglomerations are different and have a random distribution. For those specimens tested in this work, the maximum one is about 2 mm and the minimum one is 0.5 mm. The cavity formed due to liquid degeneration appears obviously in figure 6(B), denoted by the white arrow. Their average size is 0.5 mm. There are some microstructures found in the malignant tumour, such as fibre fortification (see figure 6(C)). These fortifications result from uniform or asymmetric encroachment of the malignant cell along the breast duct. At the same time, the calcifications also distribute along the fibre fortification and form the stick or Y-shaped assembly as shown in figure 6(C). In addition, some breast ducts are expanded (the black arrow in figure 6(C)). These irregular structures and special symptoms of the tissue can play very important roles in distinguishing the malignant and benign tumours.

4.4. Rocking curve

The rocking curve which can be used to study the dynamic processes of x-ray diffraction is related to the absorption, the extinction, the mosaic domain in crystals, and so on. In DEI experiments, the shape of the rocking curve is decided by the analyser Si (1 1 1) crystal and the experimental specimen (see figure 7). As listed in table 1, the peak remains in the same position but in general the sample affects the broadening of the rocking curve and also the integrated intensity.

Due to the differences between the absorption and refraction of the specimens, the DEI images let us see various microstructures clearly. The integrated intensities of the rocking curve are obviously different for different kinds of breast tissues, although its peak position and the width stay almost unchanged. The difference of integrated intensity mainly results from the differences in absorption of breast tissues under test. Because of the compactness and the relatively high density of healthy tissues, the integrated intensity for normal breast tissue is the lowest, which reflects a strong absorption. For the tumour tissues, the formation of cavities in benign tumours will increase the transmittance and result in a growth of the integrated intensity of the rocking curve. In contrast the assembling of calcified spots in the progression to cancer of diseased tissue will increase the absorption and then lead to a fall of the rocking curve. This general trend is in accordance with our earlier work in which the infrared absorption of healthy or diseased human tissues was studied (Liu *et al* 2006). We found that the IR absorption spectrum varies from abundantly featured to faint from normal breast tissue to benign tumours; while it develops from a relatively smooth spectrum to a much more complicated one in progressing to cancer of the diseased tissue. The reason for these changes is the variation of the absorption of different breast tissues in the IR region. However, the change of integrated intensity of rocking curves among different breast tissues is due to their different absorptions in the x-ray region.

5. Conclusions

DEI images can disclose the inside microstructures of various breast tissues without the need of large numbers of pathology slices. The refraction images can show the microstructures of normal, benign and malignant breast tissues with the best clarity and highest contrast in all kinds of DEI images. The peak images have higher contrast than the apparent absorption images and can show microstructures inside the breast tissues as well. There are more

abundant microstructures in the peak images recorded by x-ray films and magnified by optical microscope, but this image processing procedure is not as convenient as using CCDs. The differences of the integrated intensity of rocking curves are also a possible way to distinguish normal, benign or malignant breast tissues. The DEI method could be valuable in the diagnosis of breast cancers in their early stage. To our knowledge, so far only breast tissue specimens have been imaged with DEI, not the whole *in vivo* tissue. While DEI may be useful in characterizing breast tissue specimens, it is not yet useful in detecting breast cancer in asymptomatic women.

Acknowledgments

This work was supported by the National Natural Science Foundation of China (no. 10105002) and National Basic Research Programme of China (no. 2005CB523306).

References

- Bothorel S, Meunier B B and Muller S A 1997 Fuzzy logic based approach for semilogical analysis of microcalcification in mammographic images *Int. J. Intell. Syst.* **12** 819–48
- Chapman D, Thomlinson W, Johnston R E, Washburn D, Pisano E, Gmur N, Zhong Z, Menk R, Arfelli F and Sayers D 1997 Diffraction enhanced x-ray imaging *Phys. Med. Biol.* **42** 2015–25
- Giammarile F and Bremond A 2004 Diagnostic of breast cancer: what do clinicians expect from PEM *Nucl. Instrum. Methods Phys. Res. A* **527** 83–6
- Feig S A 2002 Effect of service screening mammography on population mortality from breast carcinoma *Cancer* **95** 451–7
- Fiedler S, Bravin A, Keyrilainen J, Fernandez M, Suortti P, Thomlinson W, Tenhunen M, Virkkunen P and Karjalainen-Lindsberg M-L 2004 Imaging lobular breast carcinoma: comparison of synchrotron radiation DEI-CT technique with clinical CT, mammography and histology *Phys. Med. Biol.* **49** 175–88
- Fiedler S, Pagot E, Cloetens P, Bravin A, Baruchel J, Hartwig J, Coan P, Salicru B and Thomlinson W 2003 Evaluation of the phase contrast techniques: diffraction enhanced imaging and propagation *Proc. SPIE* **5030** 266–73
- Freedman G M *et al* 2003 Routine mammography is associated with earlier stage disease and greater eligibility for breast conservation in breast carcinoma patients age 40 years and older *Cancer* **98** 918–25
- Hasnah M O, Zhong Z, Oltulu O, Pisano E, Johnston R E, Sayers D, Thomlinson W and Chapman D 2002 Diffraction enhanced imaging contrast mechanisms in breast cancer specimens *Med. Phys.* **29** 2216–21
- Humphrey L L, Helfand M, Chan B K S and Woolf S H 2002 Breast cancer screening: a summary of the evidence for the U.S. preventive services task force *Ann. Intern. Med.* **137** 347–60
- Lewis R A *et al* 2002 Diffraction enhanced imaging: improved contrast, lower dose x-ray imaging *Proc. SPIE* **4682** 286–97
- Lewis R A 2004 Medical phase contrast x-ray imaging: current status and future prospects *Phys. Med. Biol.* **49** 3573–83
- Liu C L, Zhang Y, Zhang X Y, Yang W T, Peng W J, Shi D R, Zhu P P, Tian Y L and Huang W X 2005 X-rays diffraction enhanced imaging of uterine leiomyomas *Med. Sci. Monit.* **11** MT33–38
- Liu C L, Zhang Y, Yan X H, Zhang X Y, Li C X, Yang W T and Shi D R 2006 Infrared absorption of human breast tissues *in vitro* *J. Lumin.* **119–200** 132–6
- Margaritondo G and Meuli R 2003 Synchrotron radiation in radiology: novel x-rays sources *Eur. Radiol.* **13** 2633–41
- Menk R H 1999 Interference imaging and its application to material and medical imaging *Nucl. Phys. B* **78** 604–9
- Niklason L T *et al* 1997 Digital tomosynthesis in breast imaging *Radiology* **205** 399–406
- Orel S G, Mendonca M H, Reynolds C, Schnall M D, Solin L J and Sullivan 1997 MR imaging of ductal carcinoma *in situ* *Radiology* **202** 413–20
- Shankar P M, Reid J M, Ortega H, Piccoli C W and Goldberg B B 1993 Use of non-Rayleigh statistics for identification of tumors in ultrasonic B-scans of the breast *IEEE Trans. Med. Imaging* **12** 687–92
- Suortti P and Thomlinson W 2003 Medical application of synchrotron radiation *Phys. Med. Biol.* **48** R1–35
- Wilkinson S J, Rogers K D, Hall C J, Lewis R A, Round A, Pinder S E, Boggis C and Hufton A 2005 Small angle diffraction imaging for disease diagnosis *Nucl. Instrum. Methods Phys. Res. A* **548** 135–9
- Zhong Z, Thomlinson W, Chapman D and Sayers D 2000 Implementation of diffraction enhanced imaging experiments: at the NSLS and ASP *Nucl. Instrum. Methods Phys. Res.* **450** 556–68